AIAA 2003-3139

Mode-matching Strategies in Slowly Varying Engine Ducts

N.C. Ovenden and S.W. Rienstra
Eindhoven University of Technology
Eindhoven, NL

9th AIAA/CEAS Aeroacoustics Conference
12-14 May 2003
Hilton Head, South Carolina

AIAA 2003-3139

MODE-MATCHING STRATEGIES IN SLOWLY VARYING ENGINE DUCTS

Nick C. Ovenden* & Sjoerd W. Rienstra†

Department of Mathematics and Computing Science,
Eindhoven University of Technology,
The Netherlands

Abstract

A matching method is proposed to connect the CFD source region to the CAA propagation region of rotor-stator interaction sound produced in a turbofan engine. The method is based on a modal decomposition across three neighbouring axial interfaces adjacent to the matching interface. The modal amplitudes are determined by a least-squares fit. By taking slowly varying modes the interface may be positioned in a duct section of varying cross section. Furthermore, the spurious reflections back into the CFD domain, which result from imperfect reflection-free CFD boundary conditions, can be filtered out by including both left- and right-running modes in the matching. Although the method should be applicable to a wider range of acoustic models, it is implemented and favourably tested for the recently available relatively simple case of slowly varying modes in homentropic potential flow in lined ducts. Homentropic potential flow is a very relevant model for the inlet side, and a good model for the bypass side if swirl or other types of vorticity are not dominant in the mean flow. By matching with density or pressure perturbations any contamination of residual non-acoustical vorticity is avoided.

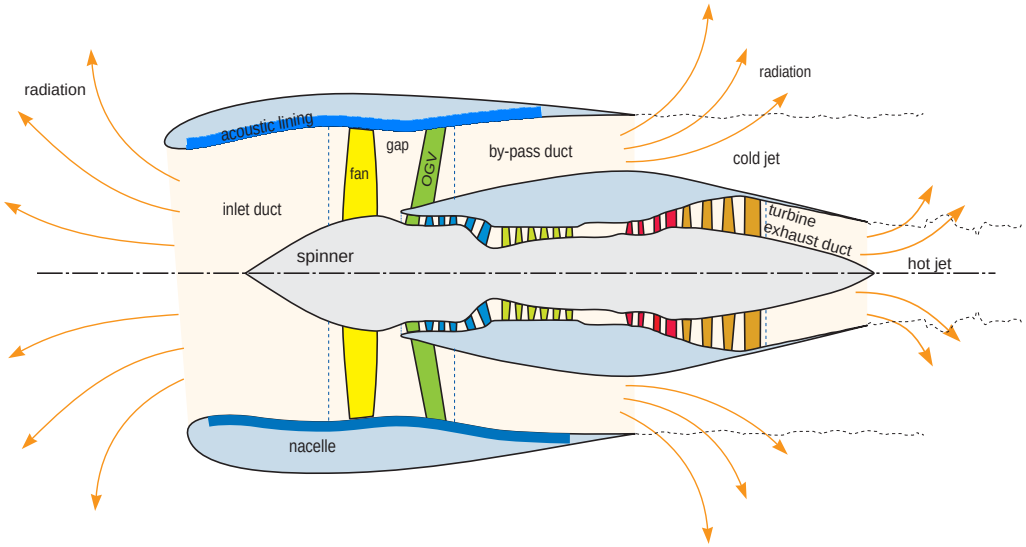

Figure 1. The zones in a typical high-bypass ratio turbofan engine

Introduction

Computationally it is inefficient, and practically as yet impossible, to describe the sound field, which is produced within a turbofan aero-engine duct by rotor-stator interaction of fan and OGVs, throughout the entire domain of interest by the same model.

In the aerodynamic regions of the source, *i.e.* in the vicinity of fan, gap, and OGV (figure 1), the unsteady parts of all flow variables such as pressure, velocity, density and possibly the thermodynamic variables are of the same order of magnitude as the steady

*Postdoctoral Research Associate. AIAA Member †Associate Professor. AIAA Member

(time-averaged) parts. The governing model is therefore nonlinear, time-dependent, and rotational. It is described by some form of the compressible Navier-Stokes equations, possibly supplemented by a turbulence model. Especially in the acoustically most critical case of heavy blade loading, this model is mathematically so complicated that it can only be solved numerically by CFD methods. On the other hand, in the acoustic regions of inlet and bypass duct and free field, the unsteady components are small compared to the steady (mean) flow. The model here may be split up into a steady description of the mean flow and a separate linear model for the perturbations. In addition, other simplifications that do not seriously affect the sound propagation may be justified, such as the absence of viscosity, vorticity and entropy variations for instance. The acoustic field may therefore be resolved by more efficient CAA or (semi-)analytical techniques.

At the interface between both models, the source data from one is to be handed over to the other. Ideally, we would want to impose continuity of all variables and their derivatives at this interface. This is, however, not possible and the differences between the models causes a matching problem across the interface where the following issues have to be faced:

1. **Inconsistent field variables.** Pressure, density and velocity satisfy different equations in different models. So, for example, a pressure-velocity field consistent in one model may be just impossible to satisfy in the other. We may have to choose which variable is preferred, and cannot have both to be true.
2. **Residual numerical errors and spurious reflections.** The numerically obtained source field may have residual errors. In particular the assumed reflection-free boundary condition is usually imperfect, and the field available from the CFD solution at the interface will in reality only partly transmit due to some reflections. This reflected part should be recognized, otherwise the resolved field will be an overestimation of reality.
3. **False reflections.** When the difference in models is too great, this will in itself create false reflections that should *not* be included. This is an additional effect to the numerical reflections noted in item 2 above. From our experience at present, the imperfect reflection-free boundary condition of 2 appears to be most significant.
4. **False near field.** A perfect matching of the acoustic field to the given field at the interface is, at least in one variable, always possible, but this solution will almost certainly contain an acoustic near field that is completely an artefact of the method. In terms of duct modes, this is the field associated with the exponentially decaying cut-off modes. If the duct near the matching interface is smooth and the field is nearly linear, this part of the modal spectrum (the amplitudes of the cut-off modes) should be small in reality, because the acoustic field's origin will be at the fictitious source distribution consisting of the rotor/stator blades and the nonlinear flow upstream, not locally. It is, however, impossible to quantify how small these modes should actually be, given the uncertainties of the source field. Therefore, we must try to limit these cut-off modes in a sensible way, but at the same time bear in mind their contribution to the flow-field.

In order to translate the aerodynamic source data into their acoustic equivalents, the following two methods have been considered by Wilson[1;2] and Nijboer & Schulten[3] respectively:

(i) **Wave splitting.** If the interface is at a section of the duct that is parallel to the axis, while the mean flow is axially constant, the field can be solved by a sum of modes. By applying conditions of continuity of at least two variables (pressure and axial velocity, pressure and pressure gradient; this depends on the acoustic model), a linear system can be created that defines the modal amplitudes. The advantage of the method is that it is relatively flexible to assumptions made about the source, so long as modes can be constructed. The disadvantages are that the duct has to be locally straight, and that care must be taken that the two field variables are not inconsistent in the acoustic model, either because of the model differences or by the numerical discretisation error.

(ii) **Ffowcs Williams-Hawkings integrals over the blades.** It is argued that in the absence of shock waves associated to the rotor or stator blades, and in the absence of an important displacement effect due to the thickness of the blades, the dominating part of the source is the pressure distribution over the blades. These constitute a rotating distribution of dipoles, of which the radiated sound can be described by a Ffowcs Williams-Hawkings integral over the blades. The advantage of this method is that the pressure distribution can probably be relatively accurately determined. The disadvantages are that the Green's function in the duct is required for the solution, which is only explicitly available for simple ducts and mean flows, while the scattering of the rotor field by the stator, and vice versa, is not included.

Triple-plane pressure matching method

The above considerations brought us to the following matching method.

In order to be able to capture any type of source, we followed the idea of mode splitting at the interface, which allows us at the same time to remove any spurious reflections in the CFD data. We assume a circular symmetric annular duct, which is perfectly reasonable near the rotor. By using the slowly varying modes of Rienstra[4;5], we are able to avoid the restriction of a straight duct section and, therefore, it is possible to match half-way along the spinner (in the inlet duct). In the present implementation, these modes are solutions of a homentropic potential flow model. The generalisation to modes in flow with swirl[6;7;8;9;10] may be a next step, but is not done here yet.

The matching is done for a single variable in order to avoid any inconsistency. A convenient choice is the pressure because this is always available, while it is (practically) not affected by vortical contamination, which cannot be absorbed by a potential flow model. This is because convected relative density (ρ) perturbations only depend on the solenoidal part of the velocity ($\boldsymbol{v}$),

$$\rho^{-1}\big(\tfrac{\partial}{\partial t} + \boldsymbol{v}\cdot\nabla\big)\rho = -\nabla\cdot\boldsymbol{v},$$

while for isentropic perturbations, pressure and density fields are merely algebraically related.

As matching of a single variable at a single axial plane is not enough to distinguish left- from right-running waves, the number of matching planes is extended to three. Two would be just enough of course, but three offers some excess of information that allows, via a least squares fit, a smoothing of errors and a better use of available information. Of course, one could take more matching planes than three; the idea remains exactly the same. Another advantage of a geometrically spread matching zone, is the possibility of limiting the amplitudes of the cut-off modes in a simple and systematic way without any resorting to ad-hoc assumptions about the *actual* source locations (see below).

The mean flow of the potential flow model is necessarily nearly uniform along a cross section. The axial velocity, mean density and mean sound speed are therefore chosen such that their cross sectional average is equal to the corresponding CFD mean flow component.

Finally, it may be noted that the present slowly varying modes are also valid for lined ducts, via the implementation of Myers' soft-wall boundary condition[11]. Hence, the matching interface may be chosen equally in either a hard-walled or lined duct section.

Equations for ideal fluid motion

As the interface refers to a jump in model, it is important to make clear what assumptions and approximations are made in our acoustic model, which forms the basis for the matching method. This will be explained in detail below.

For pressure p, density ρ, velocity vector $\boldsymbol{v}$, deviatoric stress tensor $\boldsymbol{\tau}$, temperature T, entropy s and heat flux vector $\boldsymbol{q}$ the equations for conservation of mass, momentum and energy of an ideal gas read[12]

$$\begin{aligned}\big(\tfrac{\partial}{\partial t} + \boldsymbol{v}\cdot\nabla\big)\rho &= -\rho\nabla\cdot\boldsymbol{v},\\ \rho\big(\tfrac{\partial}{\partial t} + \boldsymbol{v}\cdot\nabla\big)\boldsymbol{v} &= -\nabla p + \nabla\cdot\boldsymbol{\tau},\\ \rho T\big(\tfrac{\partial}{\partial t} + \boldsymbol{v}\cdot\nabla\big)s &= -\nabla\cdot\boldsymbol{q} + \boldsymbol{\tau}:\nabla\boldsymbol{v}.\end{aligned}$$

The variables are thermodynamically related with enthalpy h, internal energy ϵ and sound speed c by

$$\begin{gathered}T\,\mathrm{d}s = \mathrm{d}\epsilon + p\mathrm{d}\rho^{-1} = \mathrm{d}h - \rho^{-1}\mathrm{d}p,\quad h = \epsilon + p\rho^{-1},\\ p = \rho\mathcal{R}T,\quad \mathrm{d}\epsilon = C_V\mathrm{d}T,\quad \mathrm{d}h = C_P\mathrm{d}T,\\ \mathrm{d}s = C_V\frac{\mathrm{d}p}{p} - C_P\frac{\mathrm{d}\rho}{\rho},\quad c^2 = \Big(\frac{\partial p}{\partial\rho}\Big)_s = \gamma\mathcal{R}T,\\ \mathcal{R} = C_P - C_V,\quad \gamma = C_P/C_V,\end{gathered}$$

where $\mathcal{R}$ is a gas constant. For a perfect gas, the specific heats C_V (at constant volume) and C_P (at constant pressure) are constants, such that we can integrate the expression above to obtain

$$s = C_V\log p - C_P\log\rho,\quad c^2 = \gamma p/\rho.$$

In acoustics, the variations are too quick for heat conduction (Péclet number is large) while the viscous shearing forces are small (Reynolds number is large), leading to

$$\begin{aligned}\tfrac{\partial}{\partial t}\rho + \nabla\cdot\big(\rho\boldsymbol{v}\big) &= 0,\\ \rho\big(\tfrac{\partial}{\partial t} + \boldsymbol{v}\cdot\nabla\big)\boldsymbol{v} &= -\nabla p,\\ \big(\tfrac{\partial}{\partial t} + \boldsymbol{v}\cdot\nabla\big)s &= 0.\end{aligned}$$

The last equation denotes a constant entropy along streamlines. If this constant is the same for all streamlines, the flow is homentropic. If the flow is irrotational (like in the inlet), we can introduce a velocity potential ϕ with $\boldsymbol{v} = \nabla\phi$ and integrate the momentum equation to obtain Bernoulli's equation

$$\frac{\partial\phi}{\partial t} + \frac{1}{2}|\boldsymbol{v}|^2 + \frac{c^2}{\gamma-1} = G(t),$$

where G is an unimportant function of time. The flow can now be split up into a mean flow plus small perturbations

$$\begin{aligned} \boldsymbol{v} &:= \boldsymbol{V} + \boldsymbol{v}, \qquad p := P + p, \\ \phi &:= \Phi + \phi, \qquad \rho := D + \rho, \end{aligned}$$

(while a sound speed perturbation serves no purpose, so we write $c := C$) and, after linearisation, we obtain for the mean flow field (dimensionless, of course)

$$\nabla\cdot(D\boldsymbol{V}) = 0, \quad \gamma P = D^\gamma, \quad C^2 = \gamma P/D = D^{\gamma-1},$$
$$\frac{1}{2}|\boldsymbol{V}|^2 + \frac{C^2}{\gamma-1} = E, \quad \text{a constant},$$

and for the acoustic field

$$\frac{\partial}{\partial t}\rho + \nabla\cdot(D\nabla\phi + \rho\boldsymbol{V}) = 0,$$
$$\frac{\partial}{\partial t}\phi + \boldsymbol{V}\cdot\nabla\phi + p/D = 0, \quad p = C^2\rho,$$

which simplifies to solving

$$\Big(\frac{\partial}{\partial t} + \boldsymbol{V}\cdot\nabla\Big)\Big[C^{-2}\Big(\frac{\partial}{\partial t} + \boldsymbol{V}\cdot\nabla\Big)\phi\Big] = D^{-1}\nabla\cdot\big(D\nabla\phi\big).$$

Slowly varying modes

When a slowly varying duct, given by

$$R_1(X) \le r \le R_2(X), \quad X = \varepsilon x,$$

where ε is a small parameter, is the only cause of variation of the mean flow (this is an assumption), the mean flow variables depend essentially on the slow axial variable X, rather than on x, and application of the method of slow variation[13] leads to the asymptotic expansion

$$\begin{aligned} \boldsymbol{V}(X, r; \varepsilon) &= U(X)\boldsymbol{e}_x + \varepsilon V(X, r)\boldsymbol{e}_r + \mathcal{O}(\varepsilon^2), \\ D(X, r; \varepsilon) &= D(X) + \mathcal{O}(\varepsilon^2), \\ C(X, r; \varepsilon) &= C(X) + \mathcal{O}(\varepsilon^2), \\ P(X, r; \varepsilon) &= P(X) + \mathcal{O}(\varepsilon^2), \end{aligned}$$

where $\boldsymbol{e}_x$ and $\boldsymbol{e}_r$ are unit vectors in the axial and radial directions respectively. The leading-order mean flow field satisfies the equations

$$U(X) = \frac{F}{D(X)\big(R_2(X)^2 - R_1(X)^2\big)},$$
$$\frac{1}{2}U(X)^2 + \frac{1}{\gamma-1}D(X)^{\gamma-1} = E.$$

The two parameters F and E determine the entire mean flow field and must be chosen to fit the CFD mean flow data as ideally as possible. The mean flow from the CFD must therefore be stripped of any swirling and vortical component to make the velocity nearly uniform axially. Given that πF is the mass flux through an axial plane, F can be found by finding the average mass flux of the mean flow at the three axial planes given. The Bernoulli constant E can be found by a similar averaging process of the mean density or, indeed, the mean pressure or mean sound speed if they are regarded as more suitable.

Once a mean flow consistent with the acoustic model and *close* to the steady part of the CFD data has been derived, the acoustic field is Fourier-decomposed in frequency and circumferential order. If $p(\boldsymbol{x}, t)$ is periodic in time with period $2\pi/\Omega$, it can be written as

$$p(x, r, \theta, t) = \sum_{n=-\infty}^{\infty}\sum_{m=-\infty}^{\infty} p_m(x, r; n\Omega)\,\mathrm{e}^{\mathrm{i}n\Omega t - \mathrm{i}m\theta}$$

and each Fourier component is given by

$$p_m(x, r; n\Omega) = \frac{\Omega}{4\pi^2}\int_0^{2\pi}\int_0^{2\pi/\Omega} p(x, r, \theta, t)\,\mathrm{e}^{\mathrm{i}m\theta - \mathrm{i}n\Omega t}\,\mathrm{d}t\mathrm{d}\theta.$$

As we will deal in the rest of this paper with a single Fourier component $p_m(x, r; \omega)$ only, no explicit reference will be made to the circumferential order m or frequency ω dependence.

Each component is now a wave propagating in a slowly varying medium (both geometry and mean flow are to leading order functions of X only). This can be approximated by an application of the WKB method (a variant of the method of multiple scales) where each radial mode is assumed to adapt itself to the varying surroundings, without any intermodal coupling[4]. The resulting field can then be written as a summation of left- and right-running modes in the following way

$$p(x, r) = \sum_{\mu=-\infty}^{\infty} A_\mu\psi_\mu(X, r)\,\mathrm{e}^{-\mathrm{i}\int^x k_\mu(\varepsilon\sigma)\mathrm{d}\sigma}, \quad (1)$$

where $\mu = 0$ is excluded. The functions ψ_μ represent the basis functions for the right-running ($\mu > 0$) and left-running ($\mu < 0$) slowly-varying pressure modes which take the form[4]

$$\psi_\mu(X, r) = -\mathrm{i}D(X)\big(\omega - k_\mu(X)U(X)\big)$$
$$\big[N_\mu(X)\,\mathrm{J}_m(\alpha_\mu(X)r) + M_\mu(X)\,\mathrm{Y}_m(\alpha_\mu(X)r)\big], \quad (2)$$

where J_m and Y_m are Bessel functions of order m. The slowly-varying radial eigenvalues α_μ are found from the hard or soft wall boundary condition[11] and the axial eigenvalues k_μ can be subsequently derived for each

α_μ via a slowly varying dispersion relation (with the right sign convention of the square root for right, *i.e.* $\mu > 0$, and left, *i.e.* $\mu < 0$, running modes). The functions N_μ and M_μ, which are determined by a solvability condition, dictate how the modal amplitude changes axially through the duct and can be suitably normalized.

The matching method in detail

Suppose that at three axial planes $x = x_0$, x_1 and x_2 (where $x_0 < x_1 < x_2$), representing the matching zone, the pressure $p(x, r)$ can be written by a finite sum of each plane's slowly varying basis functions as follows:

$$p(x,r) = \sum_{\mu=-M}^{M} A_\mu \psi_\mu(X,r)\, \mathrm{e}^{-\mathrm{i}\int_{x_0}^{x} k_\mu(\varepsilon\sigma)\mathrm{d}\sigma}. \quad (3)$$

Hence, given the Fourier-decomposed (ω, m)-component of the pressure data $\mathcal{P}_0(r)$ at $x = x_0$, $\mathcal{P}_1(r)$ at $x = x_1$ and $\mathcal{P}_2(r)$ at $x = x_2$, we can write

$$\sum_{\mu=-M}^{M} A_\mu \psi_\mu(X_0,r) = \mathcal{P}_0(r), \quad (4a)$$

$$\sum_{\mu=-M}^{M} A_\mu \psi_\mu(X_1,r)\, \mathrm{e}^{-\mathrm{i}\int_{x_0}^{x_1} k_\mu(\varepsilon\sigma)\mathrm{d}\sigma} = \mathcal{P}_1(r), \quad (4b)$$

$$\sum_{\mu=-M}^{M} A_\mu \psi_\mu(X_2,r)\, \mathrm{e}^{-\mathrm{i}\int_{x_0}^{x_2} k_\mu(\varepsilon\sigma)\mathrm{d}\sigma} = \mathcal{P}_2(r). \quad (4c)$$

Evidently, it will not be possible to find amplitudes A_μ that satisfy this over-determined set of equations exactly. However, a best fit may be determined by a least squares approach, although some care is needed to prevent exponentially large terms at the zone ends from unbalancing the least squares minimisation. The diagram in figure 2 shows two modes approaching the three-plane interface from either side. If these modes are cut-off, $\mathrm{Im}(k_\mu) \neq 0$, then their respective amplitudes will decay exponentially as they pass through the interfaces. Hence, if they both have amplitudes of $\mathcal{O}(1)$ at the plane x_0, then at $x = x_2$ the amplitude of the right-running cut-off mode will be exponentially small and the amplitude of the left-running mode will be exponentially large. This leads to an imbalance in the minimisation process, where the cut-off modal amplitudes are in general too large, and the errors do not become spread evenly across all the axial planes. A typical consequence of this can be the appearance of oscillations or *wiggles* in the CAA pressure and velocity fields.

One satisfactory solution to the problem is to rescale the left- and right-running amplitudes and, reciprocally, rescale the corresponding basis functions, at whichever axial plane they take their maximum value in the least squares procedure. In other words, they are rescaled to the axial plane nearest their apparent source. Hence, in our diagram, the amplitude of the left-running mode is rescaled to be $\mathcal{O}(1)$ at the end interface x_2 and to be exponentially small at $x = x_0$. Note that this does not involve any manual adaptation or post-processing of the amplitudes. We just temporarily redefine amplitudes and basis functions such that the penalty in the least squares method becomes effectively much greater for cut-off modes at the outer axial planes.

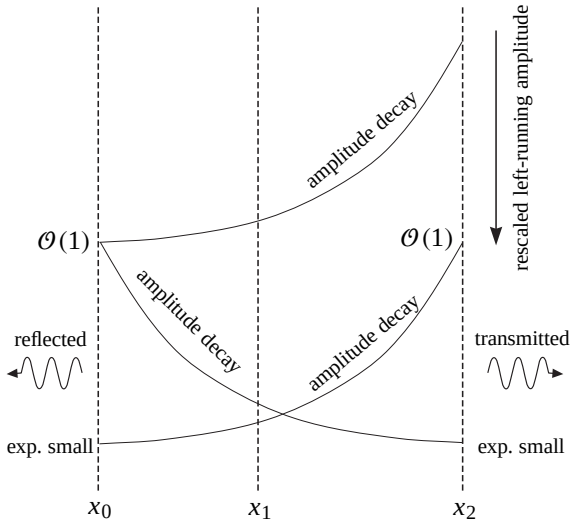

Figure 2. Sketch of the amplitude decay of cut-off modes across three axial planes.

The bonus of this rescaling is that while it limits the cut-off modes within the matching zone, it suppresses in a simple and systematic way the false near field created at the zone, but never suppresses more than what is actually present in reality.

The rescaling for the left-running amplitudes is conveniently given by introducing new amplitudes and basis functions as follows.

$$B_\mu = \begin{cases} A_\mu & \text{if } \mu > 0, \\ A_\mu\, \mathrm{e}^{-\mathrm{i}\int_{x_0}^{x_2} k_\mu(\varepsilon\sigma)\mathrm{d}\sigma} & \text{if } \mu < 0, \end{cases} \quad (5a)$$

$$\xi_\mu(r) = \begin{cases} \psi_\mu(X_0,r) & \text{if } \mu > 0, \\ \psi_\mu(X_0,r)\, \mathrm{e}^{-\mathrm{i}\int_{x_2}^{x_0} k_\mu(\varepsilon\sigma)\mathrm{d}\sigma} & \text{if } \mu < 0, \end{cases} \quad (5b)$$

$$\zeta_\mu(r) = \begin{cases} \psi_\mu(X_1, r)\, \mathrm{e}^{-\mathrm{i}\int_{x_0}^{x_1} k_\mu(\varepsilon\sigma)\mathrm{d}\sigma} & \text{if } \mu > 0, \\ \psi_\mu(X_1, r)\, \mathrm{e}^{-\mathrm{i}\int_{x_2}^{x_1} k_\mu(\varepsilon\sigma)\mathrm{d}\sigma} & \text{if } \mu < 0, \end{cases} \tag{5c}$$

$$\chi_\mu(r) = \begin{cases} \psi_\mu(X_2, r)\, \mathrm{e}^{-\mathrm{i}\int_{x_0}^{x_2} k_\mu(\varepsilon\sigma)\mathrm{d}\sigma} & \text{if } \mu > 0, \\ \psi_\mu(X_2, r). & \text{if } \mu < 0. \end{cases} \tag{5d}$$

Consequently, a more balanced system is obtained:

$$\sum_{\mu=-M}^{M} B_\mu \xi_\mu(r) = \mathcal{P}_0(r), \tag{6a}$$

$$\sum_{\mu=-M}^{M} B_\mu \zeta_\mu(r) = \mathcal{P}_1(r), \tag{6b}$$

$$\sum_{\mu=-M}^{M} B_\mu \chi_\mu(r) = \mathcal{P}_2(r). \tag{6c}$$

The least squares procedure can now be applied as follows. Multiply left and right hand sides of equations (6) with the respective complex conjugated basis functions ξ_ν^*, ζ_ν^*, and χ_ν^*, and integrate across the duct to obtain

$$\sum_{\mu=-M}^{M} B_\mu \int_{R1}^{R2} \xi_\mu(r)\xi_\nu^*(r) r\, \mathrm{d}r = \int_{R1}^{R2} \mathcal{P}_0(r)\xi_\nu^*(r) r\, \mathrm{d}r, \tag{7a}$$

$$\sum_{\mu=-M}^{M} B_\mu \int_{R1}^{R2} \zeta_\mu(r)\zeta_\nu^*(r) r\, \mathrm{d}r = \int_{R1}^{R2} \mathcal{P}_1(r)\zeta_\nu^*(r) r\, \mathrm{d}r, \tag{7b}$$

$$\sum_{\mu=-M}^{M} B_\mu \int_{R1}^{R2} \chi_\mu(r)\chi_\nu^*(r) r\, \mathrm{d}r = \int_{R1}^{R2} \mathcal{P}_2(r)\chi_\nu^*(r) r\, \mathrm{d}r, \tag{7c}$$

or in matrix form,

$$\mathcal{M}\boldsymbol{a} = \boldsymbol{p}_0, \quad \mathcal{N}\boldsymbol{a} = \boldsymbol{p}_1, \quad \mathcal{Q}\boldsymbol{a} = \boldsymbol{p}_2, \tag{8}$$

where

$$\{\mathcal{M}\}_{\nu\mu} = \int_{R_1}^{R_2} \xi_\mu(r)\xi_\nu^*(r) r\, \mathrm{d}r, \tag{9a}$$

$$\{\mathcal{N}\}_{\nu\mu} = \int_{R_1}^{R_2} \zeta_\mu(r)\zeta_\nu^*(r) r\, \mathrm{d}r, \tag{9b}$$

$$\{\mathcal{Q}\}_{\nu\mu} = \int_{R_1}^{R_2} \chi_\mu(r)\chi_\nu^*(r) r\, \mathrm{d}r, \tag{9c}$$

$$\{\boldsymbol{p}_0\}_\nu = \int_{R_1}^{R_2} \mathcal{P}_0(r)\xi_\nu^*(r) r\, \mathrm{d}r, \tag{9d}$$

$$\{\boldsymbol{p}_1\}_\nu = \int_{R_1}^{R_2} \mathcal{P}_1(r)\zeta_\nu^*(r) r\, \mathrm{d}r, \tag{9e}$$

$$\{\boldsymbol{p}_2\}_\nu = \int_{R_1}^{R_2} \mathcal{P}_2(r)\chi_\nu^*(r) r\, \mathrm{d}r, \tag{9f}$$

$$\{\boldsymbol{a}\}_\mu = B_\mu. \tag{9g}$$

The least squares approach aims to find a set of amplitudes $\boldsymbol{a}$ that minimizes the cost function

$$\left\|\mathcal{M}\boldsymbol{a} - \boldsymbol{p}_0\right\|^2 + \left\|\mathcal{N}\boldsymbol{a} - \boldsymbol{p}_1\right\|^2 + \left\|\mathcal{Q}\boldsymbol{a} - \boldsymbol{p}_2\right\|^2. \tag{10}$$

If we search for the vector $\boldsymbol{a}$ that minimizes the above cost function (10) and use the hermitian property of $\mathcal{M}$, $\mathcal{N}$ and $\mathcal{Q}$ we get* the following equation for $\boldsymbol{a}$,

$$\left(\mathcal{M}^2 + \mathcal{N}^2 + \mathcal{Q}^2\right)\boldsymbol{a} = \mathcal{M}\,\boldsymbol{p}_0 + \mathcal{N}\,\boldsymbol{p}_1 + \mathcal{Q}\,\boldsymbol{p}_2. \tag{11}$$

This equation is easily solved by standard numerical techniques. The actual reflected amplitudes A_μ for $\mu < 0$ are then recovered from the resulting B_μ after the error minimisation is completed.

To exclude the reflected modes in the above analysis is easy: all that is needed is to change the summation limits from

$$\sum_{\mu=-M}^{M} \quad \text{to} \quad \sum_{\mu=1}^{M}.$$

and restrict the set of basis functions to the ones that are outgoing. The problem remains identical, except that the size of the vectors and matrices are M and $M \times M$ respectively.

Testing the TPP matching strategy

The method was tested in a number of cases kindly provided by partners of the European collaborative project "TurboNoiseCFD". We present here some examples supplied by Rolls-Royce and DLR.

*Introduce the complex vectorial inner product $[\boldsymbol{x}, \boldsymbol{y}]$, which is equal to the ordinary inner product with $\boldsymbol{y}$ complex conjugated: $[\boldsymbol{x}, \boldsymbol{y}] = (\boldsymbol{x}, \boldsymbol{y}^*)$. Then the hermitian property of $\mathcal{M}$ implies $[\mathcal{M}\boldsymbol{x}, \boldsymbol{y}] = [\boldsymbol{x}, \mathcal{M}^*\boldsymbol{y}] = [\boldsymbol{x}, \mathcal{M}\boldsymbol{y}]$. Each squared distance in the cost function (10) becomes now like $\left\|\mathcal{M}\boldsymbol{a} - \boldsymbol{p}\right\|^2 = [\mathcal{M}\boldsymbol{a} - \boldsymbol{p}, \mathcal{M}\boldsymbol{a} - \boldsymbol{p}] = [\mathcal{M}^2\boldsymbol{a}, \boldsymbol{a}] - [\boldsymbol{a}, \mathcal{M}\boldsymbol{p}] - [\mathcal{M}\boldsymbol{p}, \boldsymbol{a}] + [\boldsymbol{p}, \boldsymbol{p}]$. If we vary around $\boldsymbol{a}$ by substituting $\boldsymbol{a} + \varepsilon\boldsymbol{b}$, we find for $O(\varepsilon)$ that the variation of $\left\|\mathcal{M}\boldsymbol{a} - \boldsymbol{p}\right\|^2$ is $2\,\mathrm{Re}\{[\mathcal{M}^2\boldsymbol{a} - \mathcal{M}\boldsymbol{p}, \boldsymbol{b}]\}$. If we look for stationary values of cost function (10) for any vector $\boldsymbol{b}$, the result (11) for $\boldsymbol{a}$ is obtained.

Rolls-Royce Fan/OGV in bypass duct

The Rolls-Royce CFD test data is based on a realistic engine geometry (figure 3) used in the TurboNoiseCFD project for investigating noise generated by rotor/stator interaction. Clearly, the engine duct geometry varies significantly along its axis, but in the region of the duct behind the stator (psogvex), the duct is more-or-less parallel, with radial variations of $\mathcal{O}(10^{-4}\,\mathrm{m})$.

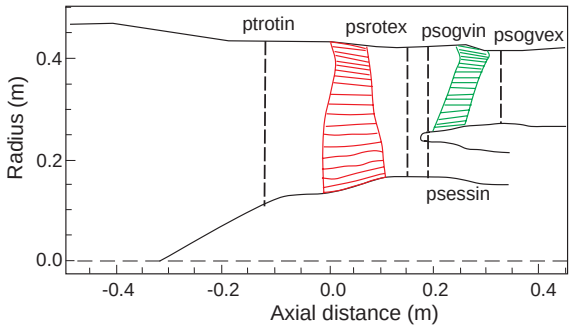

Figure 3. Fan/OGV testcase engine geometry. Rolls-Royce supplied ten axial planes located at the stator-to-bypass-duct interface (psogvex). The duct has hard walls.

Rolls-Royce supplied data for ten axial planes equally spaced between $x = 0.320$ and $x = 0.360$ at the stator-to-bypass-duct interface. Perturbation data was provided for a single frequency, $ka = 40.89$ (2BPF), and a single circumferential wavenumber, $m = -13$.

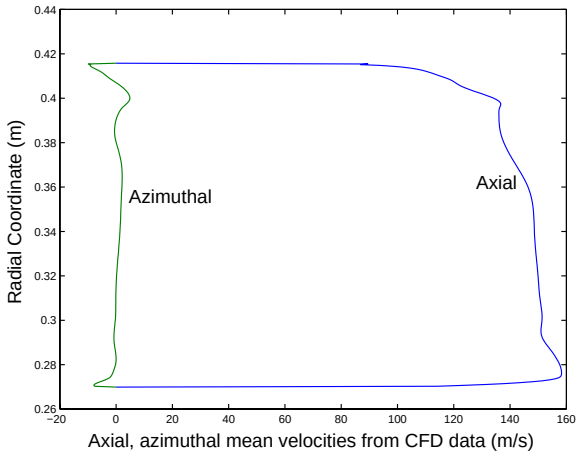

Figure 4. Bypass Fan/OGV testcase. Axial and azimuthal mean flow profiles at $x = 0.340$ m.

Observe in figure 4 that the mean flow has hardly any swirl but contains vorticity (as expected). Stripping this mean flow to create a uniform flow leads to a mean axial Mach number of $M = 0.44$ and the average hub-to-tip ratio across the interfaces is 0.649. Solving the eigenvalue problem for the acoustic model predicts five cut-on radial modes to be present. Using the supplied CFD perturbation data, traditional wavesplitting methods mentioned in the introduction of imposing continuity of pressure (ignoring reflections) and of imposing continuity of pressure and axial velocity, described as the $[P+V]$ method, were compared to the TPP matching strategy across all ten axial locations. Amplitudes for each radial mode were obtained from each of these methods as the mode's SPL (sound pressure level) at the outer casing. These results are presented in figures 5 to 8 and the main observations are described below.

On performing the matchings, it soon became clear that there is significant vorticity contamination of the velocity field and just as significant reflections in this case. The results in figure 5 for the TPP method, for instance, indicate that the reflected amplitudes of the cut-on modes are about 20% of the amplitude of their transmitted counterparts. Matching without reflections in this case therefore leads to a significant overestimation (as expected) of the transmitted acoustic field.

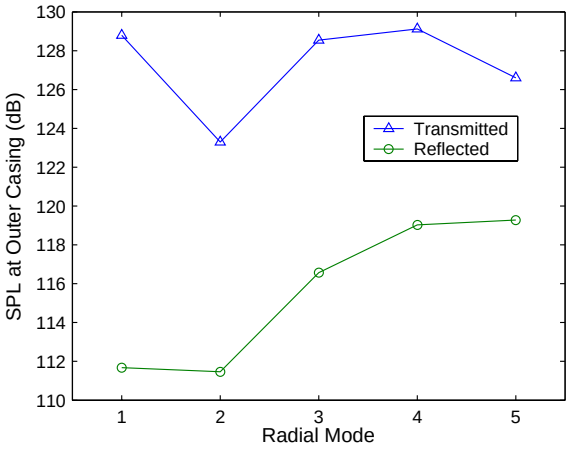

Figure 5. Bypass Fan/OGV testcase. Transmitted and reflected modal amplitudes (SPL) at the outer casing predicted by the TPP matching method at $x = 0.348$ m.

The strength of the vortical part of the flow field compared to the acoustical (irrotational) part can be clearly seen by reconstructing *irrotational* axial velocity profiles from the obtained modal amplitudes using the CAA model and comparing these to the original CFD data. In the homentropic potential flow model, the irrotational axial velocity $\frac{\partial}{\partial x}\phi$ can be obtained from the axial velocity modes $\{u_\mu\}$ that correspond to the pressure modes of the form (2). To the order of the

approximation, the axial velocity modes are given by

$$u_\mu(X,r) = \frac{k_\mu(X)\psi_\mu(X,r)}{D(X)\big(\omega - U(X)k_\mu(X)\big)}. \qquad (12)$$

These are translated to the required axial plane x, before summing them to give the complete profile (at the current frequency and circumferential wavenumber of interest). The real parts of such reconstructed axial velocity profiles from traditional $[P+V]$ wavesplitting and the TPP matching method compared at a single axial plane are shown in figure 6. The most striking observation one can make from the profiles is that the TPP strategy, which uses no velocity information, can only predict, and hence only support, (irrotational) velocity perturbations one tenth of the magnitude of the ones observed in the data.

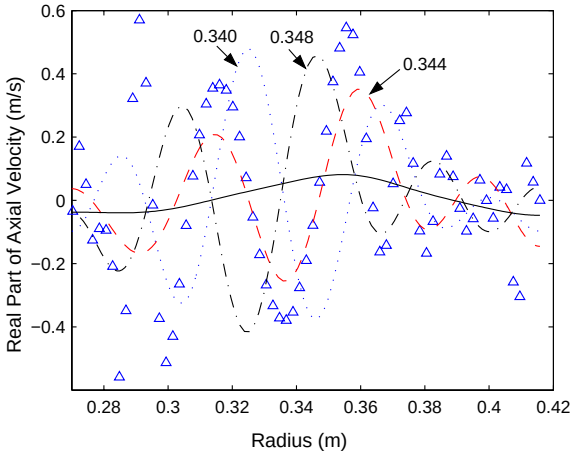

Figure 6. Bypass Fan/OGV testcase. Reconstructed axial velocity profiles (real parts) from traditional $[P+V]$ wavesplitting methods applied to data at each of the three neighbouring planes $x = 0.340$ m, $x = 0.344$ m and $x = 0.348$ m (dotted lines) and from the TPP matching method applied across all three planes (solid line). Using the homentropic potential flow model, the reconstructed profiles are all compared at the plane $x = 0.344$ m to the original CFD velocity data (triangles).

The observation that the vortical part of the axial velocity perturbations is greater than the solenoidal part naturally affects the accuracy of the traditional $[P+V]$ wavesplitting methods significantly. The axial velocity profiles from performing a $[P+V]$ wavesplitting at each neighbouring plane in figure 6, disagree with one another's solution when compared at a chosen plane because they assume a solenoidal behaviour in the velocity. Yet further evidence can be seen in the plot of transmitted modal SPL at the outer casing derived by applying the $[P+V]$ wavesplitting at five different axial locations in figure 7. Given that the amplitudes of the cut-on modes should be constant in the homentropic potential flow acoustic model, the amplitudes obtained from the traditional wavesplitting method show an enormous variability, even to the order of $10-15$ dB for the fourth and fifth radial modes. Indeed the resolution of the higher order cut-on modes appears to be strongly affected by the vorticity contamination.

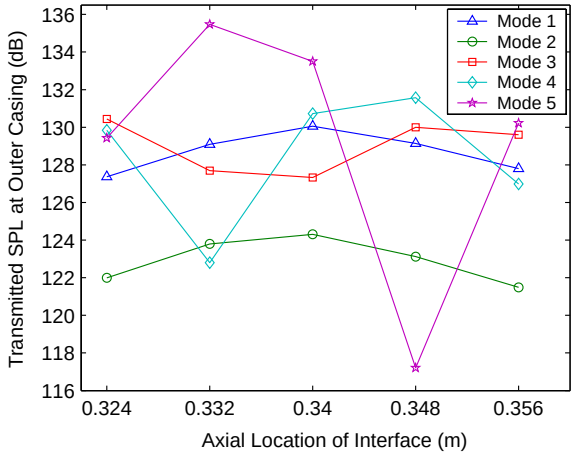

Figure 7. Bypass Fan/OGV testcase. Amplitudes (SPL) at the outer casing of the transmitted radial modes predicted by traditional $[P+V]$ wavesplitting methods at five different axial locations.

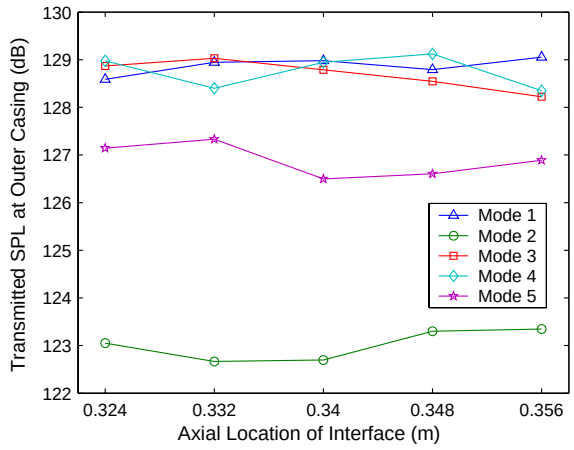

Figure 8. Bypass Fan/OGV testcase. Amplitudes (SPL) at the outer casing of the transmitted radial modes predicted by the TPP matching method at five different axial locations.

The comparison of the [P+V] wavesplitting modal amplitudes to the almost constant transmitted amplitudes, with differences much less than 1 dB, obtained by the TPP matching method (figure 8) seems to be strong proof of the superior ability of the TPP match-

ing method to capture and extract the *acoustically behaving* part of such a complicated CFD solution extremely well. The TPP matching method, in effect, has not only matched the data but synchronised the two models, leading to a greater confidence that the model jump is not too severe in this case.

As a final comparison of matching in the bypass duct case (figure 9), another set of CFD data produced for the same bypass geometry was matched using the TPP matching method and compared to a Rolls-Royce in-house wavesplitting method[1;2] and the acoustic analogy approach of Ffowcs Williams-Hawkings[3]; both of these methods were briefly described in the introduction.

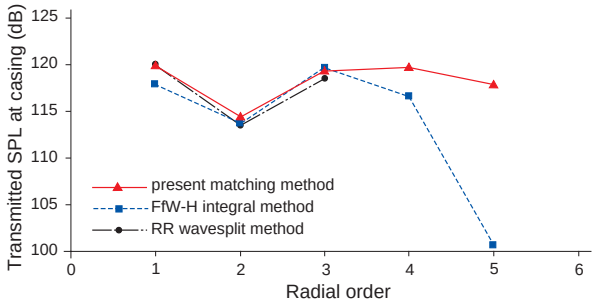

Figure 9. Bypass Fan/OGV testcase. Comparison of the TPP matching method with an in-house wavesplitting method and the acoustic analogy approach of Ffowcs Williams-Hawkings.

Very good agreement is obtained for the first three radial modes in all cases, although the agreement is nowhere near as good for the fourth and fifth radial modes. Indeed, the in-house wavesplitting method is unable to resolve these higher-order radial modes, possibly due to the strong vorticity effects described above. The TPP matching method does not suffer from such difficulties and, due to the indirectness of the acoustic analogy method and the consistency of our results, it is reasonable to postulate that the TPP result is probably the most accurate in obtaining the fourth and fifth modal amplitudes.

DLR Inlet matching on a spinner

For exactly the same engine geometry as the Rolls-Royce case (figure 3), another partner in the TurboNoiseCFD project, DLR of Germany, were able to supply sets of CFD data at three axial planes for inlet-duct matching (at location *ptrotin* in the figure). The case presented here is at a frequency of $ka = 21.5$ (1BPF) and circumferential wavenumber $m = -26$, where the average axial Mach number is taken to be $M = 0.35$. This testcase enabled us not only to tackle the difficult task of matching on the spinner, where the axial variation of the duct is highly significant, but also to examine the ability of the TPP matching method to deal with cut-off modes correctly (there are no cut-on radial modes in this case).

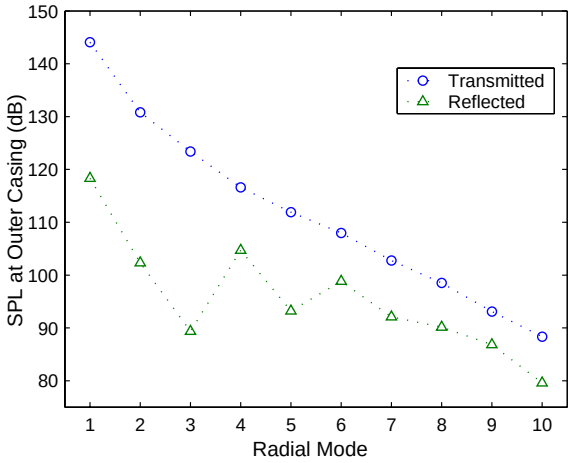

Figure 10. Inlet testcase. Transmitted and reflected modal amplitudes (SPL) at the outer casing from TPP matching.

Data was supplied at axial planes $x = -0.06$, $x = -0.05$ and $x = -0.04$ and the transmitted and reflected modal amplitudes (SPL) at the outer casing of the plane furthest upstream are shown in figure 10. Modal reflections appear to be fairly negligible in this case (20 dB lower than the transmitted amplitudes for lower radial orders) and the modal amplitudes drop

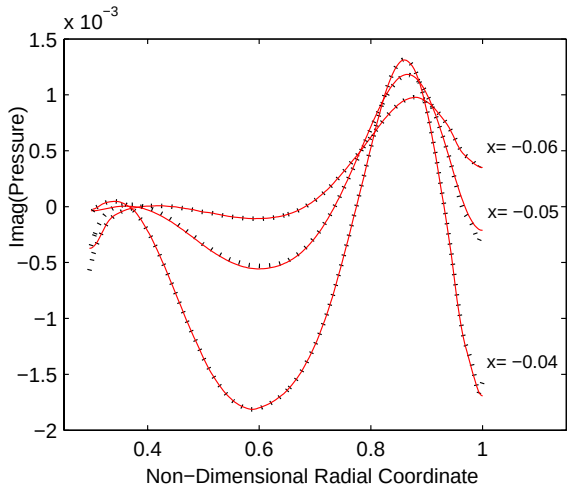

Figure 11. Inlet testcase. Comparison of CFD imaginary pressure data (dotted lines) with the modal solutions derived from the TPP matching method (solid lines) at all three axial planes - first 50 radial modes included.

smoothly with increasing radial order, in line with physical expectations.

The final figure (figure 11) shows a comparison of the CFD pressure data (imaginary part) with that derived from our homentropic potential flow model, using the obtained modal amplitudes. The agreement appears to be excellent, with both CFD and analytical models capturing the exponential decay of the sound field away from the source.

Conclusions

In order to make progress in the prediction of turbomachinery noise by direct calculation with CFD methods of the noise sources, like rotor-stator interaction between fan and OGV or between compressor and turbine stages, it is necessary to decouple the noise generation from the propagation effects. Otherwise, the available computational resources will be not sufficient for many years to come.

By our Triple-Plane Pressure (TPP) matching method, we have shown that it is possible to take the CFD noise field from planes in the vicinity of the CFD domain boundaries and extract in a robust manner the information required to input to CAA or analytical models, which are designed to describe the propagation and radiation processes more efficiently.

The method is both robust and flexible, as it is based on a least squares fit that in principle allows the matching of any flow variable at any number of planes. A subtle scaling of the amplitudes proves to be sufficient to suppress the exponential coupling of cut-off modes between the matching zone ends, and at the same time limits in a simple and systematic manner the occurrence of the false near field that is bound to occur when a pressure distribution at a single interface acts as an acoustic boundary condition.

By using slowly varying modes, there is no geometrical restriction to the location of the interface. It is indeed possible to apply the matching at any diverging or converging part of the duct. Perhaps the only locations that should be avoided for matching are close to areas where either cut-on cut-off transition (in hard-walled ducts) or near cut-on cut-off transition (in lined ducts) of a mode may occur[14;15].

Acknowledgement

This work was supported by the TurboNoiseCFD European collaborative project (EU Technical Officer: Per Kruppa, Co-ordinator: Brian Tester). We would like to thank all partners for their contributions and comments in the development of this work. We gratefully acknowledge Rolls-Royce (UK) and DLR (Germany) for supplying the CFD data presented here, and especially John Coupland (RR) for the comparison with the NLR Ffowcs Williams-Hawkings integral method of Nijboer & Schulten and the wave splitting method of Alec Wilson (RR).

References

[1] A.G. WILSON, A Method for Deriving Tone Noise Information from CFD Calculations on the Aeroengine Fan Stage, presented at the NATO RTO-AVT Symposium on Developments In Computational Aero- And Hydro-Acoustics, Manchester, UK, 8-11 October 2001

[2] A.G. WILSON Application of CFD to wake/aerofoil interaction noise - a flat plate validation case. *AIAA 2001-2135*, 2001.

[3] R.J. NIJBOER, J.B.H.M. SCHULTEN, project commissioned by Rolls-Royce, UK.

[4] S.W. RIENSTRA, 1999, Sound Transmission in Slowly Varying Circular and Annular Ducts with Flow, *Journal of Fluid Mechanics* **380**, 279–296.

[5] S.W. RIENSTRA, W. EVERSMAN, 2001, A Numerical Comparison Between Multiple-Scales and FEM Solution for Sound Propagation in Lined Flow Ducts, *Journal of Fluid Mechanics* **437**, 367 – 384.

[6] A.J. COOPER, N. PEAKE, Propagation of unsteady disturbances in a slowly varying duct with mean swirling flow, *J. Fluid Mech.*, **445**, 207–234, 2001

[7] V.V. GOLUBEV, H.M. ATASSI, Sound propagation in an annular duct with mean potential swirling flow, *Journal of Sound and Vibration*, **198** (5), p. 601–616, 1996.

[8] V.V. GOLUBEV, H.M. ATASSI, Acoustic-vorticity waves in swirling flows, *Journal of Sound and Vibration*, **209** (2), p. 203–222, 1998.

[9] C.K.W. TAM, L. AURIAULT The wave modes in ducted swirling flows, *Journal of Fluid Mechanics*, **371**, p. 1–20, (*AIAA-98-2280*), 1998.

[10] R.J. NIJBOER Eigenvalues and eigenfunctions of ducted swirling flows, *AIAA Paper 2001-2178*, 7th AIAA/CEAS Aeroacoustics Conference, Maastricht, The Netherlands, May 28-30, 2001 *(NLR-TP-2001-141)*.

[11] M.K. MYERS On the acoustic boundary condition in the presence of flow. *J. Sound Vib.*, **71**(3), 429-434, 1980.

[12] L.D. LANDAU AND E.M. LIFSHITZ, Fluid Mechanics, 2nd edition, Pergamon Press, Oxford, 1987.

[13] M. VAN DYKE, *Slow Variations in Continuum Mechanics*, in: Advances in Applied Mechanics, Volume 25, pp. 1-45, Academic Press, Orlando, 1987.

[14] S.W. RIENSTRA Cut-on, cut-off transition of sound in slowly varying flow ducts. *Aerotechnica - Missili e Spazio, special issue in memory of Prof D.G. Crighton*, **79**, nos. 3-4, 93-97. (edited by L. Morino and N. Peake), 2000.

[15] N.C. OVENDEN Near cut-on/cut-off transition in lined ducts with flow. *AIAA 2002-2445*, 8th AIAA/CEAS Aeroacoustics conference, 17-19 June 2002, Breckenridge, Colorado, 2002.